Reconfigurable Optical Computer for Solving Partial Differential Equation

by Chen Shen

B.S in Optoelectronic Science and Technology, July 2016, Shenzhen University

A Thesis submitted to

The Faculty of
The School of Engineering and Applied Science
of The George Washington University
in partial fulfillment of the requirements
for the degree of Master of Science

January 10, 2020

Thesis directed by

Volker J. Sorger
Associate Professor of Engineering and Applied Science

Acknowledgements

First, I would express my thanks to Professor Volker J. Sorger for teaching me with extraordinary knowledge and experience, also giving me a wonderful research opportunity as a master student. Also, I would like to thank all the members of the group. They shared the new ideas, suggestions, and comments with me especially Dr. Mario Miscuglio, who gives me opportunities to ask any scientific question anytime and tutors me with great patience. I have asked him many questions and he has answered even more. Last, here, I would also thank the staffs in The George Washington University (GW) Nanofabrication and Imaging Center (GWNIC).

Abstract of Thesis

Reconfigurable Optical Computer of Solving Partial Differential Equation

Nowadays, digital processors are overwhelmed by vast data and complex iterative operation. Thus, some of the workloads can be taken by more specific processor whose hardware is engineered to map specific functionalities and operations such as TPU and FPGAs. In this category, various photonic engines[1] which leverage on the absence of RC delay, distributed network and possibility to do weighted addition inherently by interference and concurrently exploit attojoule efficient high-speed modulators. Here we introduce Reconfigurable Optical Computer (ROC), a research project undertaken by Professor Volker J. Sorger' OPEN Lab Team and professor Tarek El-Ghazawi's HPCL Team both at the George Washington University, through the funding of NSF RAISE Grant. This project is mainly working on the physics theory and fabrication technology of analog co-processors in silicon photonics and optical metatronics. The goal of ROC is to investigate, model and ultimately develop an optical solution that can numerically and experimentally solve various partial differential equations (PDE).

My contribution to ROC has been to prove the reconfigurability of the photonic integrated version of ROC, by numerically modeling a programmable photonic chip in a photonic interconnect simulation framework (Lumerical-Interconnect) photonic integrated aiming to map different partial differential equation problems which describe heat transfer problems in different materials. I compared the solutions obtained at each node of photonic circuit to the discretized solutions obtained using commercially available heat transfer simulation (COMSOL) which uses finite element modeling. Since

each material has precise thermal property, the characteristic heat transfer map is uniquely represented, thus attaining a library of photonic chip configuration for solving Laplace equation applied at different domains. Therefore, the designed chip can be reprogrammed to solve Laplace heat transfer equation for different materials and holds the potential to solve other kinds of PDE.

Table of Contents

Acknowledgements ..... **ii**

Abstract of Thesis ..... **iii**

Table of Contents ..... **v**

List of Figures ..... **vi**

List of Tables ..... **vii**

List of Abbreviation ..... **viii**

Glossary of Terms ..... **x**

Chapter 1 – Towards Optical Analog Computing **1**

1.1 Gap of tradition electronic circuit 1

1.2 Partial Differential Equation (PDE) 1

1.3 Reconfigurable Optical Computer (ROC) 3

1.4 Photonic Integrated Circuit (PIC) 3

Chapter 2 – Reconfigurable part of ROC **4**

2.1 First year of ROC 4

2.2 Innovation of reconfigurability 4

2.3 My contribution to ROC project 5

2.2.3 Stage 1 Optical Mesh Building 5

2.3.2 Stage 2 Thermal simulation in COMSOL 8

2.3.3 Stage 3 Normalization and Comparison 12

2.3.4 Result 13

2.3.5. Analysis 16

Chapter 3 – Discussion **19**

3.1 Limitation of ROC 19

Whole bibliography **19**

List of Figures

Figure 1. (a)Image of node structure (b) General structure of optical simulation model. ..6

Figure 2. (a) A general structure of optical simulation (b)Image of node structure.....7

Figure 3. The geometric setting of thermal transfer simulation. 8

Figure 4. Heat transfer simulation of Zirconium.....9

Figure 5. The geometric setting of thermal transfer simulation. 10

Figure 6. The heat map of Aluminum, temperature ranging from 0K to 10^4K. 11

Figure 7. Models matched with Aluminum, Vanadium and Calbarb 13

List of Tables

Table 1. The excel file generated by python-scripted tool 13

Table 2. The error sets are input into Origin Lab software 16

List of Abbreviation

EAM

electro-absorption modulator **4**

ER

extinction ratio 5

FEM

finite element model **4**

GW

The George Washington University iv

GWNIC

The George Washington University Nanofabrication and Imaging Center..... iv

HPCL

High Perfomance Computing Laboratory..... v

InP

Indium Phosphide 3

OPEN

Orthogonal Physics Enabled Nanophotonics..... v

PDE

partial differential equation..... v

ROC

Reconfigurable Optical Computer v

SPACE

Silicon Photonic Approximate Computing Engine..... 4

S-parameter

scattering parameter 5

Glossary of Terms

Application-specific integrated circuit

An application-specific integrated circuit is an integrated circuit (IC) customized for a particular use, rather than intended for general purpose use.

Co-processor

A co-processor is a computer processor used to supplement the functions of the primary processor (the CPU). Operations performed by the coprocessor may be floating point arithmetic, graphics, signal processing, string processing, cryptography or I/O interfacing with peripheral devices. By offloading processor-intensive tasks from the main processor, coprocessors can accelerate system performance.

COMPSOL Multiphysics

COMSOL Multiphysics is a cross-platform finite element analysis, solver and multiphysics simulation software. It allows conventional physics-based user interfaces and coupled systems of partial differential equations (PDEs). COMSOL provides an IDE and unified workflow for electrical, mechanical, fluid, and chemical applications. An API for Java and LiveLink for MATLAB may be used to control the software externally, and the same API is also used via the Method Editor.

Distributed element model

In electrical engineering, the distributed element model or transmission line model of electrical circuits assumes that the attributes of the circuit (resistance, capacitance, and

inductance) are distributed continuously throughout the material of the circuit. This is in contrast to the more common lumped element model, which assumes that these values are lumped into electrical components that are joined by perfectly conducting wires. In the distributed element model, each circuit element is infinitesimally small, and the wires connecting elements are not assumed to be perfect conductors; that is, they have impedance. Unlike the lumped element model, it assumes non-uniform current along each branch and non-uniform voltage along each node. The distributed model is used at high frequencies where the wavelength becomes comparable to the physical dimensions of the circuit, making the lumped model inaccurate.

Epsilon-near-zero

The window of frequency in which the permittivity is low, i.e., near the plasma frequency, has also become a topic of research interest in several potential applications. The first attempts to build a material with low permittivity at microwave frequencies date back to several decades ago, where their use was proposed in antenna applications for enhancing the radiation directivity. Similar attempts have been presented over the past years with analogous purposes. Other more recent investigations of the properties of ε-near-zero (ENZ) materials and metamaterials and their intriguing wave interaction properties have been reported. In particular, Ref. 18 addresses and studies the possibility of designing a bulk material impedance matched with free space but whose permittivity and permeability are simultaneously very close to zero. In all these works, the main attempt has been to exploit the low-wave-number (index near zero) propagation in such materials, which might provide a relatively small phase variation over a physically long

distance in these media. When interfaced with materials with larger wave number, this implies the presence of a region of space with almost uniform phase distribution, providing the possibility for directive radiation toward the broad side to a planar interface, as proposed over past the years for antenna applications. Also, in Ref. 18, the possibility of utilizing the matched low- index metamaterial for transforming curved phase fronts into planar ones has been suggested, exploiting the matching between the aforementioned metamaterial and free space. Nader Engheta's[3] group has proposed several different potential applications of ENZ and/or μ-near-zero materials for different purposes. Relying on the directivity enhancement that such materials may provide.

Extinction ratio

The ratio $r_e = P_1/P_0$ of two optical power levels of a digital signal generated by an optical source expressed as a fraction in dB or as percentage.

Finite difference method

In mathematics, finite-difference methods (FDM) are numerical methods for solving differential equations by approximating them with difference equations, in which finite differences approximate the derivatives. FDMs are thus discretization methods. FDMs convert a linear (non-linear) ODE/PDE into a system of linear (non-linear) equations, which can then be solved by matrix algebra techniques. The reduction of the differential equation to a system of algebraic equations makes the problem of finding the solution to a given ODE ideally suited to modern computers, hence the widespread use of FDMs in modern numerical analysis[1]. Today, FDMs are the dominant approach to

numerical solutions of partial differential equations.

Indium tin oxide

Indium tin oxide (ITO) is a ternary composition of indium, tin and oxygen in varying proportions. Depending on the oxygen content, it can either be described as a ceramic or alloy. Indium tin oxide is typically encountered as an oxygen-saturated composition with a formulation of 74% In, 18% O2, and 8% Sn by weight. Oxygen-saturated compositions are so typical, that unsaturated compositions are termed oxygen-deficient ITO. It is transparent and colorless in thin layers, while in bulk form it is yellowish to grey. In the infrared region of the spectrum it acts as a metal-like mirror. Indium tin oxide is one of the most widely used transparent conducting oxides because of its two main properties: its electrical conductivity and optical transparency, as well as the ease with which it can be deposited as a thin film. As with all transparent conducting films, a compromise must be made between conductivity and transparency, since increasing the thickness and increasing the concentration of charge carriers increases the material's conductivity and decreases its transparency. Thin films of indium tin oxide are most commonly deposited on surfaces by physical vapor deposition. Often used is electron beam evaporation, or a range of sputter deposition techniques.

Lumerical INTERCONNECT

INTERCONNECT, Lumerical's photonic integrated circuit simulator, verifies multimode, bidirectional, and multi-channel PICs. Creating project in this hierarchical

schematic editor, people can use our extensive library of primitive elements, as well as foundry-specific PDK elements, to perform analysis in the time or frequency domain.

Lumped element

The lumped element model (also called lumped parameter model, or lumped component model) simplifies the description of the behavior of spatially distributed physical systems into a topology consisting of discrete entities that approximate the behavior of the distributed system under certain assumptions. It is useful in electrical systems (including electronics), mechanical multibody systems, heat transfer, acoustics, etc. Mathematically speaking, the simplification reduces the state space of the system to a finite dimension, and the partial differential equations (PDEs) of the continuous (infinite-dimensional) time and space model of the physical system into ordinary differential equations (ODEs) with a finite number of parameters.

Multigrid method

In mathematics, the conjugate gradient method is an algorithm for the numerical solution of particular systems of linear equations, namely those whose matrix is symmetric and positive-definite. The conjugate gradient method is often implemented as an iterative algorithm, applicable to sparse systems that are too large to be handled by a direct implementation or other direct methods such as the Cholesky decomposition. Large sparse systems often arise when numerically solving partial differential equations or optimization problems. The conjugate gradient method can also be used to solve

unconstrained optimization problems such as energy minimization. It was mainly developed by Magnus Hestenes and Eduard Stiefel who programmed it on the Z4. The biconjugate gradient method provides a generalization to non-symmetric matrices. Various nonlinear conjugate gradient methods seek minima of nonlinear equations.

Nanophotonics

Nanophotonics or nano-optics is the study of the behavior of light on the nanometer scale, and of the interaction of nanometer-scale objects with light. It is a branch of optics, optical engineering, electrical engineering, and nanotechnology. It often (but not exclusively) involves metallic components, which can transport and focus light via surface plasmon polaritons. The term nano-optics, just like the term optics, usually refers to situations involving ultraviolet, visible, and near-infrared light (free-space wavelengths from 300 to 1200 nanometers).

Chapter 1 – Towards Optical Analog Computing

1.1 Gap of tradition electronic circuit

Although analog electronic computing engine performs extraordinarily in digital systems for special-purpose processing because of its non-iterative operation nature, it is limited by run-time and programmability-speed[1]. Digital technology is facing the inevitable halt of Moore's law due to physical limits which constrain denser integration and the constraints given by Dennard scaling[4] on power consumption which states that as transistors get smaller, their power density stays constant, so that the power consumption stays in proportion with area. The current improvement strategy is parallelization, using multiple processors or co-processors with specific architectures which are able to efficiently perform complex or recursive operations. All these technologies still rely on electronic therefore limited by RC delay and temporization set by a <4 GHz clock.

We are using instead analog processor for solving a specific functionality which usually requires immense power consumption and lengthy when implemented on analog process. To accomplish higher processing data throughput/runtime ratio, here we demonstrate photonic integrated circuit, which enables both analog compute-hardware while exploiting time parallelism as well as capitalizing on-chip dense integration.

1.2 Partial Differential Equation (PDE)

In mathematics, a partial differential equation (PDE) that contains unknown multivariable functions and their partial derivatives. PDEs are used to formulate problems involving functions of several variables, and are either solved numerically, or used to

create a computer model. PDEs can be used to describe a wide variety of phenomena such as sound, heat, diffusion, electrostatics, electrodynamics, fluid dynamics, elasticity, gravitation and quantum mechanics[8]. These seemingly distinct physical phenomena can be formalized similarly in terms of partial differential equations. Just as ordinary differential equations often model one-dimensional dynamical systems, PDEs often model multidimensional systems and multivariable functions. PDEs find their generalization in stochastic partial differential equations[15].

For the Reconfigurable Optical Computer project, we are aiming to solve two-dimensional second-order elliptic PDEs. Regarding elliptic PDEs, setting boundary condition is significant for deriving PDEs because you can derive PDEs by applying boundary condition to the originally equations. For example, in a 2-D Laplace's equation:

$$\nabla^2 u = \frac{\partial^2 u}{\partial x^2} + \frac{\partial^2 u}{\partial y^2} = 0$$

for the geometry of a rectangle, $0 \le x \le L$ and $0 \le y \le H$, the boundary condition will be:

$$u(0, y) = g_1(y)\ u(L, y) = g_2(y)\ u(x, 0) = f_1(x)\ u(x, H) = f_2(x)$$

Then by adding these conditions to Laplace's equation, we can solve it to:

$$u(x, y) = u_1(x, y) + u_2(x, y) + u_3(x, y) + u_4(x, y)$$

Because the Laplace's equation is linear and homogeneous and each of the pieces is a solution to Laplace's equation then the sum will also be the solution. In my project, the heat transfer equation is also a second-order partial differential equation, thus we can build a analog computing engine mapping with heat transfer equation, indicating that we can solve PDE in analog computer.

1.3 Reconfigurable Optical Computer (ROC)

Reconfigurable Optical Computer (ROC) is a reconfigurable photonic accelerator, implemented in two distinct physical technologies, capable of solving PDEs through the finite difference method, constructed in a physical analog mesh which is distributed network but differing from the electrical implementation which is usually lumped circuit by performing summation of electrical displacement current for Metatronic ROC and summation of optical intensity in photonic ROC[9].

1.4 Photonic Integrated Circuit (PIC)

A photonic integrated circuit or integrated optical circuit miniaturizes multiple photonic functions and is similar to an electronic integrated circuit. [57]

The most commercially utilized material platform for photonic integrated circuit is Silicon and Indium Phosphide (InP), which allows for the integration of various optically active and passive functions on the same chip.

Chapter 2 – Reconfigurable part of ROC

2.1 First year of ROC

Our group[1] have recently established a Silicon Photonic Approximate Computing Engine (SPACE) used for solving 2D second-order elliptic PDEs. Silicon Photonic Invertible Cloverleaf Cross mesh (SPICC) is the physical implementation of a photonic mesh able to drive the optical power similarly to a lumped electrical circuit which mimics a Heat-transfer problem. The four-directional nodes in the model split the incoming light equally into three other directions simulating an optical version of Kirchhoff's Law in analogy to a uniform electronic resistive circuit. By manipulating the intensity and position of special light input, it is possible to set the boundary condition. The output at each node, was spit adding an extra drop line and the optical power was coupled out by means of grating couplers and ultimately an IR camera was used for detecting in parallel the optical power at all the output ports which represents the solution of the discretized solution given by the photonic circuit at each pint of the mesh. Furthermore, comparing with a simulated heat transfer problem using finite element model (FEM) tool which meshes the domain with the same resolution, they achieved a 97 percent accuracy PDE solution.

2.2 Innovation of reconfigurability

According to the previous work mentioned above, the approximate optical computing engine our group build is able to find accurate solutions to a PDE which is fixed for the reason that the engine fabricated is passive. Although, it is envisioned that the reconfigurability functionality can be obtained by adding electro-absorption

modulator (EAM) at each node. My goal is to proceed in this direction enabling the reprogrammable functionality to the optical computing engine. Before trying to solve different type of PDEs, our system needs to be able to map the same heat transfer equation for different domains characterized by various thermal conductivity and heat capacitance.

Besides, in our photonic computing engine, boundary conditions can also be reprogrammed for the accessibility of shining light at any node in the grid.

2.3 My contribution to ROC project

2.2.3 Stage 1 Optical Mesh Building

My initial work of ROC is building a new designed model, showing the reconfigurability of the computing engine. I choose Lumerical Interconnect software to emulate the PIC. As a first step we introduce reconfigurability, aiming to make the engine tunable, by adding modulators between neighboring nodes. Within the numerical simulation environment, the dynamic range of a modulator is translated in terms of scattering parameter matrix (S-parameter, transmittance and reflectance). In this way, we can simply tune the extinction ratio (ER) of modulator by directly altering the scattering matrix of it. For instance, if a -10dB ER modulator would be introduced, first the -10dB has to be converted to percentage, which is 10%. Since the S-parameter matrix describing an N-port (in our case, 2-port) network that will be square matrix of dimension 2 and will therefore contain 4 (2^2) elements, we need to take a square root of this 10% for S-parameter. Thus, we can input the 0.316228 as the value of s21 amplitude for S-parameter matrix in the Interconnect.

In optical simulation, a 3x3 optical mesh was built to imitate the mesh structure of heat transfer. At crossing nodes, we select another type of S-parameter to perform the optical characteristic of equal splitter. Considering every node has four directions, regardless which direction does the light propagate through this S-parameter, the light will split into other three directions with equivalent value. To implement the function of equal splitter, the matrix is read from a perfect equal splitter node file. In this file, the script was written to set the incoming light evenly into three remaining directions. We use power meter to read and record the power dropped at each node. A 1W continuous wave laser source is placed at the left top corner to generate light which mimics the BC of high local temperature. (Figure 1)

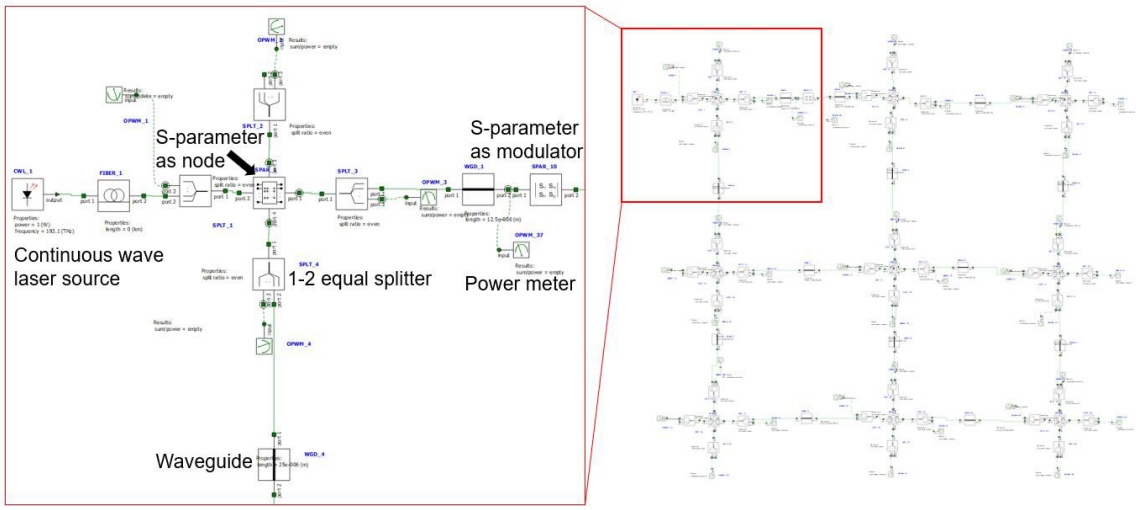

(a) (b)

Figure 1. (a)A detailed image of node structure. We can read and add the data of four power meters connected with an equal splitter around the node up to obtain the power through this node. (b) A general structure of optical simulation model, which is a 5x5 mesh. Light propagates from a continuous wave laser source located at left top corner.

The time window of whole model is set to be 500 picoseconds while the bit rate is 2.5bits/s. Also sample rate is fixed to 193.1 THz, which is also the frequency of every waveguide. Hence, number of samples is 96550, calculated by other settings above.

However, after simulation, several problems are revealed. First, the mesh size is so micro that we could not observe the heat decay slope. However, considering the simulation time boosts exponentially when mesh size increases, we can only rise the mesh size to 5x5. On the other hand, the value recorded by power meter is unstable. Therefore, we replaced it with oscilloscope, which would record the all 9998 values during the simulating process.

Here we present a new model (Figure 2), which is 5x5 size and installing oscilloscope instead of power meter.

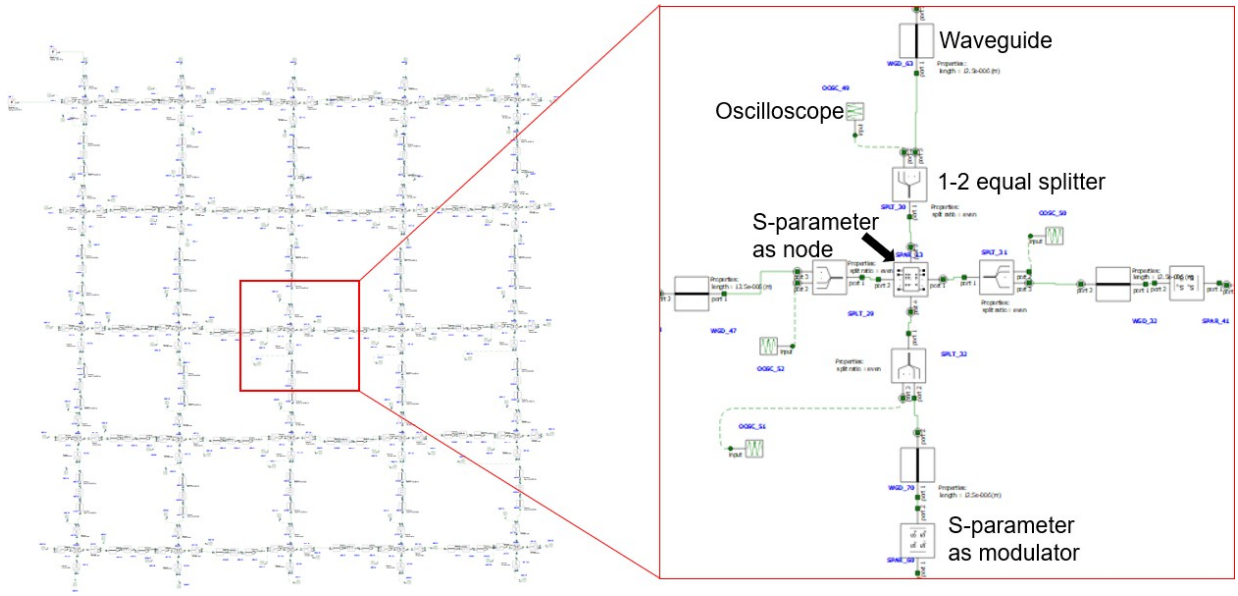

Figure 2. (a) A general structure of optical simulation model, which is a 5x5 mesh. Light propagates from a continuous wave laser source located at left top corner. (b)A detailed image of node structure. We can read and add the data of four oscilloscopes connected with an equal splitter around the node to obtain the power through this node.

Although we place modulators between every two neighboring nodes, the default extinction ratio is set to be 1, which will not have influence on light transmission because P_{in}/P_{out} ratio is also 1. These modulators will only be activated until we alter the scattering matrix parameter.

2.3.2 Stage 2 Thermal simulation in COMSOL

Next, a baseline with heat transfer simulation should be established. In COMSOL Multiphysics simulation, five materials are selected to build the thermal baselines: Aluminum, Copper, Gold, Silver, Zirconium. To study the heat map of these materials, several configurations need to be set in advance. First, geometry (figure 3): In a two-dimensional plane, one 100x100 square (default geometrical unit in COMSOL) is equally divided into 25 blocks. Meanwhile, two point are placed to form an angle at left top corner, these two sides of the angle are settled to be -173°C (100K). Simultaneously all boundaries of external square are set to be minus 273°C (0K), which is the heat sink in this model.

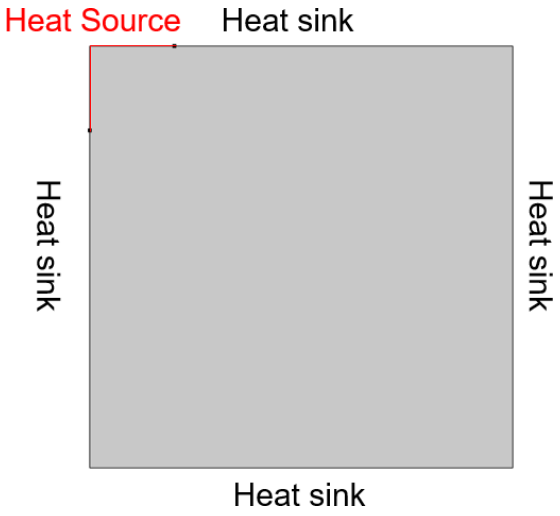

Figure 3. The geometric setting of thermal transfer simulation, a 5 by 5 square with one heat source (-173°C) at the left top corner and heat sinks (-273°C) at remaining boundaries.

After simulation, we can have a heat map like the example of the heat transfer in a Zirconium plate. To compare with optical simulation result, we need to extract 25 values from the center of 25 blocks.

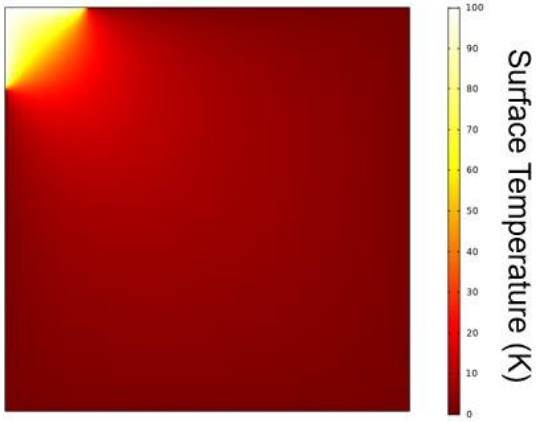

Figure 4. The heat transfer simulation of Zirconium, with heat source at left top corner while heat dissipates at boundary heat sink.

Three problems are exposed in this simulation:

1. Since the heat source is on the edge of the square, that the highest value of temperature would so be on the edge too. However, we extract thermal value from the center of smaller blocks to read and draw the heat map. Here deflection is cause because the highest value is not recorded. To solve this problem, we need to place the heat source at the center of left top block that we can accurately present the heat map of heat transfer in materials.

2. Regarding materials, because all five materials we choose are metal, the thermal properties are highly analogous. Thus, we can hardly build different PICs mapping with these metal's thermal simulation. For preventing similarity, we need to focus on materials with very different thermal conductive properties. Thus, we can have an easier comparison with the photonic engine solution.

3. The heat source temperature versus temperature of heat sink is controversial, for the reason that in COMSOL Multiphysics, thermal conductivity of various materials is calculated as a function rather than a numerical constant. According to Vosteen and

Hans-Dieter[62], the general equation for the temperature dependence of thermal conductivity can be formulated:

$$\lambda(T) = \lambda(0)0.99 + T(a - b/\lambda(0))$$

where λ is the thermal conductivity, a is the empirical constants and b is the corresponding uncertainties. By deriving the equation, we can find out that if T=0K, this equation does not hold.

In order to solve problems above, an advanced heat transfer model is made. First, three materials are selected: Aluminum, Vanadium and Calcarb CVD 20 (a new insulator material made up of carbon fiber). Geometrically, in a two-dimensional plane, one 100x100 square (default geometrical unit in COMSOL) is equally divided into 25 blocks (Figure 5). Meanwhile, a 0.1x0.1 square with its center located at the center of top left block is set be a 9727°C (10000K) heat source, simultaneously all boundaries of external square are set to be 0°C, which are the heat sink in this model.

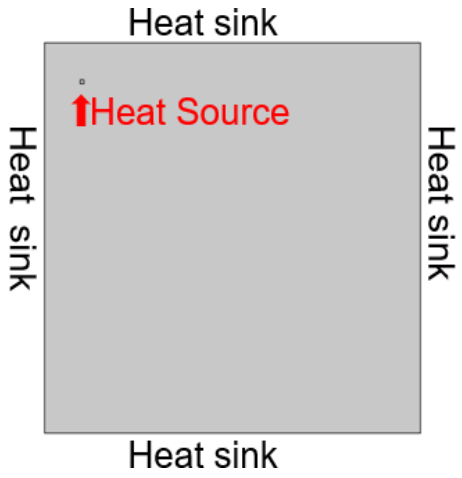

Figure 5. The geometric setting of thermal transfer simulation, which is a 5 by 5 square with one heat source (9727°C) at the left top block center and heat sinks (0°C) at boundaries.

The computing engine of thermal simulation is described by following equation:

$$d_z \rho C_p \mathbf{u} \cdot \nabla T + \nabla \cdot \mathbf{q} = d_z Q + q_0 + d_z Q_{ted} \quad (1)$$

$$\mathbf{q} = -d_z k \nabla T \quad (2)$$

Where ρ represents the density of material(kg/m^3), Q is the heat source, **u** is the velocity, **q** is the heat flux and k is the thermal conductivity(W/(m·k)). In our stationary case, d_z is out-of-plane thickness, C_p represents the specific heat capacity(J/(kg·k)), and Q_{ted} is the thermoelastic damping.

The final setting is regarding mesh size, we choose free triangular mesh type with maximum mesh size of 1 (default geometric unit in COMSOL) and minimum mesh size of 1/100. In order to achieve the heat map, the mesh size must be smaller than the minimum element size of my model, which is the heat source square. However, the simulation time would exponentially increase if the mesh size is smaller than my setting.

After computing study, the heat maps for each material are presented (figure 6). We record the thermal values of 25 points at the center of 25 square blocks. Thus, these values form a data set representing the heat transfer map of each material.

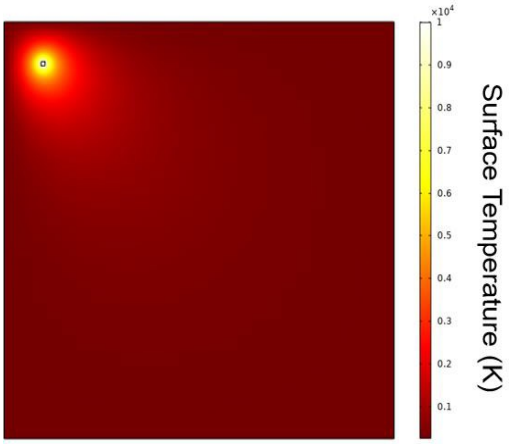

Figure 6. The heat map of Aluminum, temperature ranging from 0K to 10^4K.

2.3.3 Stage 3 Normalization and Comparison

After we achieve the data sets from both optical and thermal simulation, a normalization process needs to be applied before synchronous comparison: First part of normalization could be represented by this formula: $A_{column}=B_{column}-min(B)$, where B column is the data set before this normalization process and A column is the normalized data set. Since the sources of both thermal and optical models are at left top corner and heat/light propagate from source corner to right bottom corner, the minimum value is always the value of the right bottom corner. Then formula $C_{column}=A_{column}/(max(A)/100)$. By these procedures above we can get each data set normalized from 0 to 100. Next, we set the normalized data sets of three materials from thermal simulation as baseline, comparing with Interconnect simulation data set by subtracting each other. So that the average error can be presented after adding the errors together and dividing by 2500 (one hundred times of the amount of data in each data set). The average accuracy is one minus average error. Notably, limited by nowadays modulator technology, the maximum extinction ratio of modulator can only be set to -10dB. Because the dissipating speed in heat transfer is much faster than in optical simulation, the average accuracy is lower than 70% if the extinction ratio of all modulators is 0dB. Therefore, we can calculate the error of each model then tune the modulator of these models and make their average accuracy fixed to 70%.

To increase the calculating efficiency, I code an automatic tool with Python to normalize data set and complete comparison between optical and thermal simulation. As mentioned above in 2.3.1, the oscilloscope records 9998 values for every node, hence, in

the script I appoint the tool to extract only the order of 9000 value for its stability. The rest of the script are serving for normalization and subtracting one data set from the other one. At the end, the tool would export a excel file recording the whole processing period. The following figure is an example of one excel file.

	A	B	C	D	E	F	G	H	I
node1	0.412361	-3.84722	94.7374	100	100	0	0	28.1552	71.8448
node2	0.00162	-27.9057	70.67897	74.60514	15.58402	59.02112	59.02112	28.1552	71.8448
node3	6.88E-06	-51.6223	46.96235	49.57108	5.435494	44.13559	44.13559	28.1552	71.8448
node4	2.36E-07	-66.2627	32.32196	34.11743	1.65842	32.45901	32.45901	28.1552	71.8448
node5	8.71E-09	-80.6	17.98465	18.98369	0.240268	18.74342	18.74342	28.1552	71.8448
node6	0.00162	-27.9057	70.67897	74.60514	15.58404	59.0211	59.0211	28.1552	71.8448
node7	0.000177	-37.5295	61.05515	64.44672	14.9988	49.44791	49.44791	28.1552	71.8448
node8	8.77E-06	-50.5716	48.01304	50.68013	8.639965	42.04017	42.04017	28.1552	71.8448
node9	3.82E-07	-64.1822	34.40244	36.31347	3.783732	32.52974	32.52974	28.1552	71.8448
node10	1.63E-08	-77.8843	20.70031	21.8502	0.857157	20.99305	20.99305	28.1552	71.8448
node11	6.88E-06	-51.6223	46.96235	49.57108	5.435498	44.13558	44.13558	28.1552	71.8448
node12	8.77E-06	-50.5716	48.01304	50.68013	8.639967	42.04017	42.04017	28.1552	71.8448
node13	1.04E-06	-59.8311	38.75354	40.90627	6.514019	34.39225	34.39225	28.1552	71.8448
node14	8.51E-08	-70.7006	27.884	29.43294	3.39663	26.03631	26.03631	28.1552	71.8448
node15	5.70E-09	-82.4429	16.14173	17.03839	0.852082	16.18631	16.18631	28.1552	71.8448
node16	2.36E-07	-66.2627	32.32196	34.11743	1.658421	32.459	32.459	28.1552	71.8448
node17	3.82E-07	-64.1822	34.40244	36.31347	3.783733	32.52974	32.52974	28.1552	71.8448
node18	8.51E-08	-70.7006	27.884	29.43294	3.39663	26.03631	26.03631	28.1552	71.8448
node19	1.09E-08	-79.6079	18.97674	20.03089	1.972897	18.05799	18.05799	28.1552	71.8448
node20	1.06E-09	-89.753	8.831615	9.322205	0.475941	8.846264	8.846264	28.1552	71.8448
node21	8.71E-09	-80.6	17.98465	18.98369	0.240267	18.74342	18.74342	28.1552	71.8448
node22	1.63E-08	-77.8843	20.70031	21.8502	0.857157	20.99305	20.99305	28.1552	71.8448
node23	5.70E-09	-82.4429	16.14173	17.03839	0.852082	16.18631	16.18631	28.1552	71.8448
node24	1.06E-09	-89.753	8.831615	9.322205	0.475942	8.846264	8.846264	28.1552	71.8448
node25	1.39E-10	-98.5846	0	0	0	0	0	28.1552	71.8448

Table 1. The excel file generated by python-scripted tool and converted to pdf file, which is the accuracy of Calcarb cvd 20 comparing with one circuit. Column A is the No.9000 raw data extracted from oscilloscope output data set, which unit is W. Column B is the data from column A, converting unit to dB/m. Column C&D are the normalization process turns data set into 0-100. Column E is the 0-100 normalized data set of thermal simulation. After subtract column D by column E, we get the error distribution between two simulation. For calculating average error, we still need to take absolute number from column F preventing negative number. By adding 25 numbers in column G up and dividing them by 25, we got column H, which is the percentage of average error. Finally, subtracting 100 by the average error in column H, we can achieve the percentage of average accuracy we are figuring.

2.3.4 Result

Within the model, since we place S-parameter between every two nodes, it is accessible for us to altering the ER of every modulator in terms of replacing the S-parameter matrix calculated from power decay percentage. Initially, modulators near the

laser source is raised to maximum value ----- 10dB, simply because the dissipating speed in heat map is much rapider than in optical model. According to the file exported by comparison tool, we find out that more modulators need to be activated.

After 85 models built and adjusted, we finally match three PICs for three materials' heat transfer map. As figure 8 shown below, the models with 70% average accuracy matched with three materials' heat map are structural different.

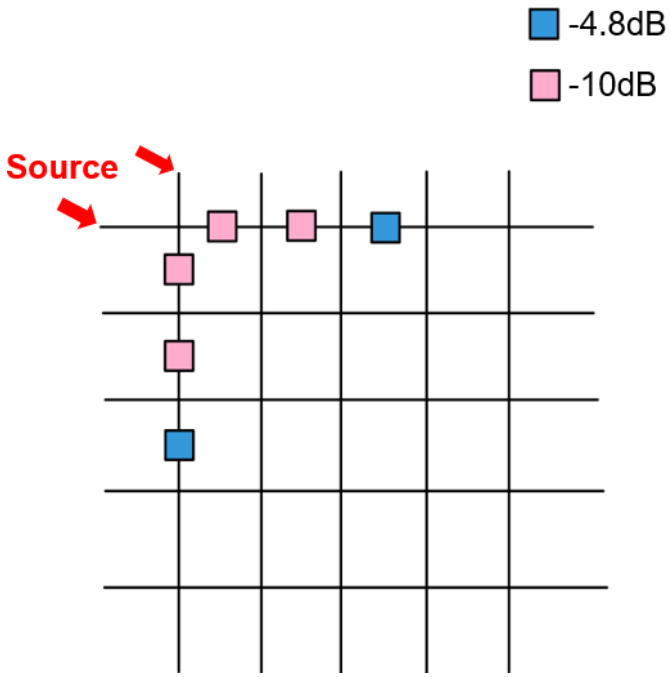

(a)

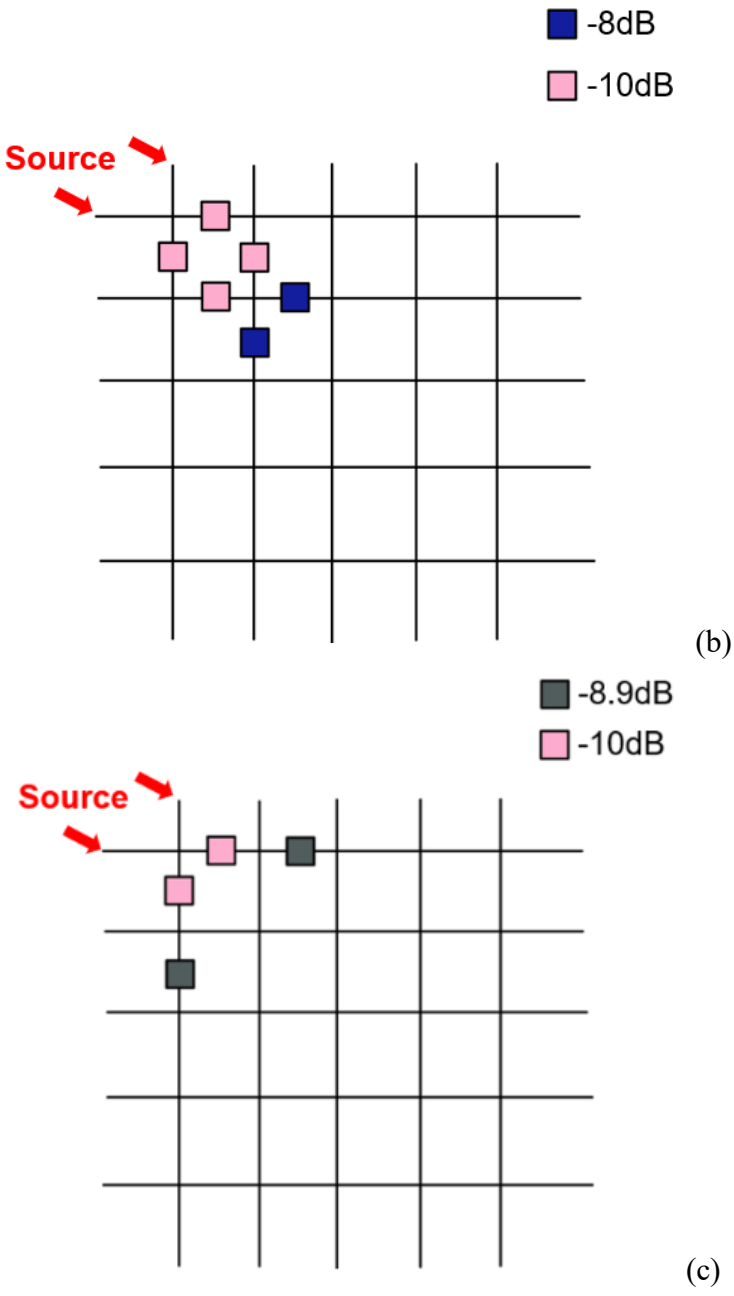

Figure 7. (a) Model matched with Aluminum. (b) Model matched with Vanadium. (c) Model matched with Calcarb.

Here we present a table on error map and average accuracy of different materials matching with different models.

Material	Model (a) Error Map and Accuracy	Model (b) Error Map and Accuracy	Model (c) Error Map and Accuracy
Aluminum	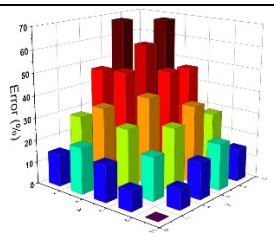 70.00%	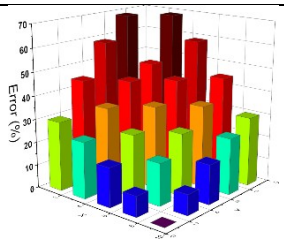 67.26%	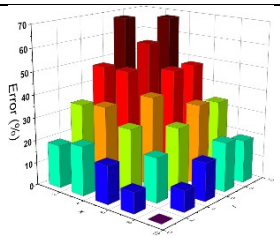 69.10%
Vanadium	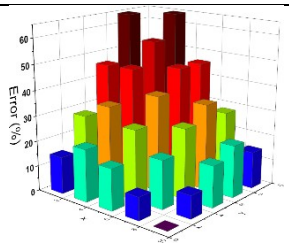 70.90%	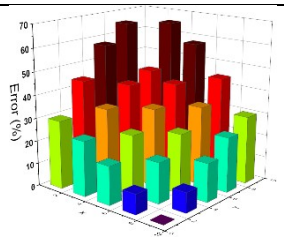 68.15%	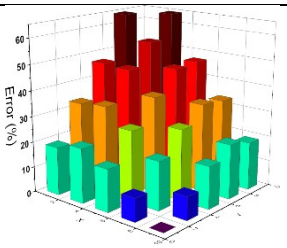 70.00%
Calcarb CVD 20	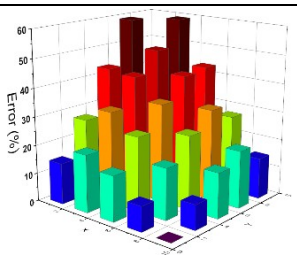 72.75%	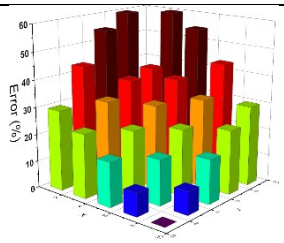 70.00%	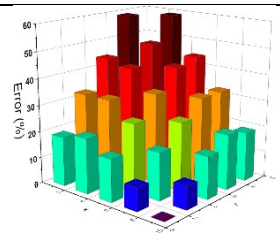 71.84%

Table 2. The error sets are input into Origin Lab software to produce the error maps. Calcarb CVD 20 has higher accuracy among three materials comparing with different circuits while Aluminum has lowest accuracy.

2.3.5. Analysis

In table 2, we can ascertain that the most considerable errors are on the first level from the source. The main reason for that is because we set a restriction on the extinction

ratio of the modulator. Specifically, limited by current technology, the maximum extinction ratio we choose in Interconnect simulation is -10dB. On the other hand, the dissipate slope in thermal simulation is exceptionally steeper. Thus, even maximum modulators are placed between source node and the first level nodes, the error after analysis is remaining nonnegligible.

Besides, in the error map, we are not able to observe the error of source node because our data set is normalized from 0 (right bottom node) to 100 (left top node). Therefore, after subtraction, the error of these two nodes equals zero.

Moreover, due to our normalization process applied on optical simulation data set, if the minimum value of data set is extremely small, which mean the power has almost fully dissipated at the right bottom corner, the gaining values of first level nodes after addition process would be exceedingly high, which causes greater error. In this case, a “free path” needs to be left for light propagating through, otherwise light will die out before it reached the right bottom corner. From another perspective, if high extinction ratio modulators are added between boundary nodes, there should be no more modulator at central “path”. Likewise, if central “path” was shut down, light should be able to propagate through boundary.

2.4 The practical meaning of my work

The design we proposed delivers a possibility to replicate the functionality of a lumped circuit model and solve PDE effortlessly and noniteratively by using finite difference approach. Although the project is still on simulation stage[1], but we restrict the circuit with modern modulation technology, that we can experimentally solve various PDE by nanofabrication. With reconfigurable part of ROC, we can now indicate that our

design is completely able to accommodate to different types of partial differential equations.

Chapter 3 – Discussion

3.1 Limitation of ROC

Theoretically, electronic circuit are lumped elements while photonic circuit is distributed network. Explicitly, in electronic circuit the wavelength of electromagnetic wave is usually larger than the footprint size of the circuit. Thus, the phase difference (delay) within the circuit is negligible that Kirchhoff's law can be applied. Therefore, a lumped circuit can solve problems with exactly 1:1 finite difference approach. On the other hand, in photonic circuit, the wavelength of light involved is normally 1550nm. In this way, the size of circuit is commonly bigger than the wavelength of light, hence Kirchhoff's law does not hold.

To sum up, in lumped circuit, local variation would cause global change within the whole circuit, while in distributed circuit, local variation would only lead to local effect. Hence, there is a fundamental gap in mapping electronic circuit and photonic circuit.

Whole bibliography

[1] Sun, S., Miscuglio, M., Kayraklioglu, E., Shen, C., Anderson, J., El-Ghazawi, T., . . . Sorger, V. J. (2019). Analog photonic computing engine as approximate partial differential equation solver.

[2] Y. Li, I. Liberal, C. Della Giovampaola, and N. Engheta, "Waveguide metatronics: Lumped circuitry based on structural dispersion," Science advances, vol. 2,

no. 6, e1501790, 2016.

[3] Nasim Mohammadi Estakhri, Nader Engheta, “Inversed-designed metastructure that solves equations”, Science, vol. 363, 2019.

[4] Robert Dennard, Andre Leblanc, “Design of Ion-Implanted MOSFET’s with Very Small Physical Dimension”. IEEE Journal of Solid-State Circuits. SC-9 (5). 1974.

[5] “International technology roadmap for semiconductors 2.0 2015 edition executive report,” ITRS, Tech. Rep., 2015.

[6] “International roadmap for devices and systems 2017 edition,” IEEE, Tech. Rep., 2017.

[7] K. Vissers, “Versal: The xilinx adaptive compute acceleration platform (acap),” in Proceedingsofthe2019ACM/SIGDAInternationalSymposiumonField-Programmable Gate Arrays, ACM, 2019, pp. 83–83.

[8] G Liebmann, “Solution of partial differential equations with a resistance network analogue,” British Journal of Applied Physics, vol. 1, no. 4, p. 92, 1950.

[9] Tarek El-Ghazawi, Volker J. Sorger, “Reconfigurable Optical Computer for Simulation of Physical Processes”, 2016

[10] J. Ramirez-Angulo and M. R. DeYong, Digitally-configurable analog vlsi chip and method for real-time solution of partial differential equations, US Patent 6,141,676, 2000.

[11] V. J. Sorger, S. Sun, T. El-ghazawi, A. h. A. Badawy, and V. K. Narayana, “Reconfigurable optical computer,” pat. 20170161417, 2017.

[12] I. H. Herron and M. R. Foster, Partial Differential Equations in Fluid Dynamics. Cambridge University Press, 2008, ISBN: 0521888247.

[13] M. N. O. Sadiku and L. C. Agba, “A simple introduction to the transmission-line modeling,” IEEE Transactions on Circuits and Systems, vol. 37, no. 8, pp. 991–999, 1990.

[14] H. Berestycki and Y. Pomeau, Nonlinear PDE’s in Condensed Matter and Reactive Flows. Dec. 2002, ISBN: 9789401003070.

[15] A. Selvadurai, Partial Differential Equations in Mechanics 1: Fundamentals, Laplace’s Equation, Diffusion Equation, Wave Equation. Apr. 2000, ISBN: 9783662040065.

[16] H.Y.J.Y.S.L.C. Tang Q. Mi, “Pde (ode)-based image processing methods for optical interferometry fringe,” 2013.

[17] E. Rocca and R. Rossi, “entropic” solutions to a thermodynamically consistent PDE system for phase transitions and damage,” SIAM Journal on Mathematical Analysis, vol. 47, no. 4, pp. 2519–2586, 2015.

[18] I. Richter, K. Pas, X. Guo, R. Patel, J. Liu, E. Ipek, and E. G. Friedman, “Memristive accelerator for extreme scale linear solvers,” in Government Microcircuit Applications & Critical Technology Conference (GOMACTech), 2015.

[19] J. Zhu, Solving Partial Differential Equations on Parallel Computers an Introduction. World Scientific Pub Co Inc, 1994, ISBN: 9810215789.

[20] L. Pinuel, I. Martin, and F. Tirado, “Aspecial-purpose parallel computer for solving partial differential equations,” pp. 509–517, 1998.

[21] J.Dongarra, “Current trends in high performance computing and challenges for the future,” AMC Learning Webinar held on February 7, 2017.

[22] P. Palmer, A. R. Copson, and S.Redshaw, “Investigations into the use of an

electrical resistance analogue for the solution of certain oscillatory-flow problems," Aero. Res. Counc. R & M, no. 3121, 1959.

[23] J. Ramirez-Angulo and M. R. DeYong, "Digitally-configurable analog vlsi chip and method for real-time solution of partial differential equations", US Patent 6,141,676, 2000.

[24] A. Hastings, The Art of Analog Layout (2ndEdition). Pearson, 2005, ISBN:0131464108.

[25] "Electronics resurgence initiative: Page 3 investments architectures thrust, hr001117s0055," Defense Advanced Research Project Agency, Tech. Rep., 2017.

[26] R. M.X. Z. V.J. Sorger N.D. Lanzillotti-Kimura, "Ultra-compact silicon nanophotonic modulator with broadband response," Nano photonics, vol. 1, no. 1, 2012.

[27] A. Mehrabian, Y. Al-Kabani, V. J. Sorger, and T. A. El-Ghazawi, "PCNNA: A photonic convolutional neural network accelerator," CoRR, vol. abs/1807.08792, 2018. arXiv: 1807.08792.

[28] S. Sun, V. K. Narayana, I. Sarpkaya, J. Crandall, R. A. Soref, H. Dalir, T. ElGhazawi, and V. J. Sorger, "Hybrid photonic-plasmonic nonblocking broadband 5 5 router for optical networks," IEEE Photonics Journal, vol. 10, no. 2, pp. 1–12, 2018.

[29] N. Mohammadi Estakhri, B. Edwards, and N. Engheta, "Inverse-designed meta structures that solve equations," Science, vol. 363, no. 6433, pp. 1333–1338, 2019.

[30] G. Tsoulos, MIMO system technology for wireless communications. CRC press, 2006.

[31] M. Hu, J. P. Strachan, Z. Li, E. M. Grafals, N. Davila, C. Graves, S. Lam, N. Ge, J. J. Yang, and R. S. Williams, "Dot-product engine for neuromorphic computing:

Programming 1t1m crossbar to accelerate matrix-vector multiplication," in Proceedings of the 53rd annual design automation conference, ACM, 2016, p. 19.

[32] M. N. Bojnordi and E. Ipek, "Memristive boltzmann machine: A hardware accelerator for combinatorial optimization and deep learning," in 2016 IEEE International Symposium on High Performance Computer Architecture (HPCA), IEEE, 2016, pp. 1– 13.

[33] H. N.V. S. J. George, "Towards on-chip optical ffts for convolutional neural networks," IEEE International Conference on Rebooting Computing (ICRC), 2017.

[34] M. Alioto, "Energy-quality scalable adaptive vlsi circuits and systems beyond approximate computing," Design, Automation —& Test in Europe Conference —& Exhibition, 2017.

[35] N. Engheta, "Circuits with light at nanoscales: Optical nanocircuits inspired by metamaterials," Science, vol. 317, no. 5845, pp. 1698–1702, 2007.

[36] N. Engheta and R. W. Ziolkowski, Metamaterials: physics and engineering explorations. John Wiley & Sons, 2006.

[37] Y.Gui, M. Miscuglio, Z.Ma, M.T.Tahersima, H.Dalir, and V.J.Sorger, "Impact of the process parameters to the optical and electrical properties of rf sputtered indium thin oxide films: A holistic approach," arXiv preprint arXiv:1811.08344, 2018.

[38] R. Amin, R. Maiti, C. Carfano, Z. Ma, M. H. Tahersima, Y. Lilach, D. Ratnayake, H. Dalir, and V. J. Sorger, "0.52 v mm ITO-based mach-zehnder modulator in silicon photonics," APL Photonics, vol. 3, no. 12, p. 126104, 2018.

[39] Z. Ma, Z. Li, K. Liu, C. Ye, and V.J.Sorger, "Indium-tin-oxide for high-performance electro-optic modulation," Nanophotonics, vol. 4, no. 1, pp. 198–213, 2015.

[40] A. Alu, V. Shalaev, M. Loncar, and V. J. Sorger, “Metasurfaces - from science to applications,” Nanophotonics, vol. 7, no. 6, pp. 949–951, 2018.

[41] M. H. Tahersima, M. D. Birowosuto, Z. Ma, W. C. Coley, M. D. Valentin, S. Naghibi Alvillar, I.-H. Lu, Y. Zhou, I. Sarpkaya, A. Martinez, et al., “Testbeds for transition metal dichalcogenide photonics: Efficacy of light emission enhancement in monomer vs dimer nanoscale antennae,” ACS Photonics, vol. 4, no. 7, pp. 1713– 1721, 2017.

[42] R.M.M. Mattheij, S. W. Rienstra, and J.H.M. ten Thije Boonkkamp, Partial Differential Equations: Modeling, Analysis, Computation (Monographs on Mathematical Modeling and Computation). Society for Industrial and Applied Mathematics,2005, ISBN: 0898715946.

[43] A. Benoit, F. Chyzak, A. Darrasse, S. Gerhold, M. Mezzarobba, and B. Salvy, “The dynamic dictionary of mathematical functions (ddmf),” in Proceedings of the Third International Congress Conference on Mathematical Software, ser. ICMS’10, Berlin, Heidelberg: Springer-Verlag, 2010, pp. 35–41, ISBN: 3-642-15581-2, 978-3-64215581-9.

[44] E. R. Vrscay, Amath 353: Partial differential equations i, 2010.

[45] J. Irwin and R. Nelms, Basic engineering circuit analysis. Hoboken, N.J: Wiley, 2015, ISBN: 978-1118992661.

[46] N. M. Estakhri, B. Edwards, and N. Engheta, “Inverse-designed metastructures that solve equations,” Science, vol. 363, no. 6433, pp. 1333–1338, 2019.

[47] J. S. Townsend, Modern Approach to Quantum Mechanics Second Edition. Univ Science Books, 2012, ISBN: 1891389785.

[48] A. Vakil and N. Engheta, “Transformation optics using graphene,” Science, vol.332, no. 6035, pp. 1291–1294, 2011.

[49] S. Yun, Z. H. Jiang, Q. Xu, Z. Liu, D. H. Werner, and T. S. Mayer, “Low-loss impedance-matched optical metamaterials with zero-phase delay,” ACSnano, vol. 6, no. 5, pp. 4475–4482, 2012.

[50] P. Moitra, B. A. Slovick, Z. Gang Yu, S. Krishnamurthy, and J. Valentine, “Experimental demonstration of a broadband all-dielectric metamaterial perfect reflector,” Applied Physics Letters, vol. 104, no. 17, p. 171102, Apr. 2014.

[51] Y. Li, S. Kita, P. Mu˜Aoz, O. Reshef, D. I. Vulis, M. Yin, M. Lon¨Aar, and E. Mazur, “On-chip zero-index metamaterials,” Nature Photonics, vol. 9, no. 11, pp. 738–742, Nov. 2015.

[52] Y. Li, I. Liberal, C. Della Giovampaola, and N. Engheta, “Waveguide metatronics: Lumped circuitry based on structural dispersion,” Science Advances, vol. 2, no. 6, 2016.

[53] Y. Li and N. Engheta, “Capacitor-inspired metamaterial inductors,” Phys. Rev. Applied, vol. 10, p. 054021, 5 2018.

[54] V. J. Sorger, N. D. Lanzillotti-Kimura, R.-M. Ma, and X. Zhang, “Ultra-compact silicon nanophotonic modulator with broadband response,” Nanophotonics, vol. 1, no. 1, pp. 17–22, 2012.

[55] R. Amin, R. Maiti, C. Carfano, Z. Ma, M. H. Tahersima, Y. Lilach, D. Ratnayake, H. Dalir, and V. J. Sorger, “0.52 V mm ITO-based Mach-Zehnder modulator in silicon photonics,” APL Photonics, vol. 3, no. 12, p. 126104, Dec. 2018.

[56] H. Dalir, F. Mokhtari-Koushyar, I. Zand, E. Heidari, X. Xu, Z. Pan, S. Sun, R.

Amin, V. J. Sorger, and R. T. Chen, “Atto-Joule, high-speed, low-loss plasmonic modulator based on a diabatic coupled waveguides,” Nanophotonics, vol. 7, no.5, pp. 859–864, 2018.

[57] R. Amin, J. George, J. Khurgin, T. El-Ghazawi, P. R. Prucnal, and V. J. Sorger, “Attojoule Modulators for Photonic Neuromorphic Computing,” in Conference on Lasers and Electro-Optics (2018), paper ATh1Q. 4, Optical Society of America, May 2018, ATh1Q.4.

[58] W. Bao, M. Melli, N. Caselli, F. Riboli, D. S. Wiersma, M. Staffaroni, H. Choo, D. F. Ogletree, S. Aloni, J. Bokor, S. Cabrini, F. Intonti, M. B. Salmeron, E. Yablonovitch, P. J. Schuck, and A. Weber-Bargioni, “Mapping Local Charge Recombination Heterogeneity by Multidimensional Nano spectroscopic Imaging,” Science, vol. 338, no. 6112, pp. 1317–1321, Dec. 2012.

[59] W. Bao, N. J. Borys, C. Ko, J. Suh, W. Fan, A. Thron, Y. Zhang, A. Buyanin, J. Zhang,S.Cabrini,P.D.Ashby,A.Weber-Bargioni,S.Tongay,S.Aloni,D.F.Ogletree, J. Wu, M. B. Salmeron, and P. J. Schuck, “Visualizing nanoscale excitonic relaxation properties of disordered edges and grain boundaries in monolayer molybdenum disulfide,” Nature Communications, vol. 6, p. 7993, Aug. 2015.

[60] N. Caselli, F. La China, W. Bao, F. Riboli, A. Gerardino, L. Li, E. H. Linfield, F. Pagliano, A. Fiore, P. J. Schuck, S. Cabrini, A. Weber-Bargioni, M. Gurioli, and F. Intonti, “Deep-subwavelength imaging of both electric and magnetic localized optical fields by plasmonic campanile nanoantenna,” Scientific Reports, vol. 5, p. 9606, Jun. 2015.

[61] C. D. Sarris, “Adaptive mesh refinement for time-domain numerical

electromagnetics," Synthesis Lectures on Computational Electromagnetics, vol. 1, no. 1, pp. 1– 154, 2007.

[62] Vosteen, H., & Schellschmidt, R. (2003). Influence of temperature on thermal conductivity, thermal capacity and thermal diffusivity for different types of rock

[63] Larry Coldren, Scott Corzine, & Milan Mashanovitch. (2012). Diode lasers and photonic integrated circuits John Wiley and Sons.

[64] Liu, A., Paniccia, M., Rong, H., Jones, R., Cohen, O., Hak, D., & Fang, A. (2005). A continuous-wave raman silicon laser. *Nature, 433*(7027), 725-728.

[65] Sawchuk, A. A., & Strand, T. C. (1984). Digital optical computing. *Proceedings of the IEEE, 72*(7), 758-779

[66] A. Alu, M. G. Silveirinha, A. Salandrino, and N. Engheta, "Epsilon-near-zero metamaterials and electromagnetic sources: Tailoring the radiation phase pattern," Physical review B, vol. 75, no. 15, p. 155410, 2007.